eng

MDPI

Article

Thermodynamic Assessment of Different Feedstocks Gasification Using Supercritical Water and CO_2 for Hydrogen and Methane Production

Luis David García Caraballo [1], Julles Mitoura dos Santos Junior [1], Icaro Augusto Maccari Zelioli [1], York Castillo Santiago [1], Juan F. Perez Bayer [2] and Adriano Pinto Mariano [1,*]

[1] Faculdade de Engenharia Química, Universidade Estadual de Campinas (UNICAMP), Av. Albert Einstein 500, Campinas 13083-852, SP, Brazil; ldavidgarciac@gmail.com (L.D.G.C.); jullesmitoura7@gmail.com (J.M.d.S.J.); i121006@dac.unicamp.br (I.A.M.Z.); yorkcastillo@id.uff.br (Y.C.S.)

[2] Grupo de Manejo Eficiente de la Energía—GIMEL, Departamento de Ingeniería Mecánica, Facultad de Ingeniería, Universidad de Antioquia—UdeA, Calle 70 No. 52-21, Medellín 050010, Colombia; jfernando.perez@udea.edu.co

* Correspondence: adpm@unicamp.br

Abstract: The supercritical water gasification (SCWG) and carbon dioxide gasification of agro-industrial and urban waste residues—Coffee Husk, Eucalyptus Biochar, Energy Sugarcane, and Refuse-Derived Fuel (RDF)—were studied using TeS® v.2 software, which employs a non-stoichiometric thermodynamic model to minimize Gibbs free energy and predict equilibrium compositions. The effects of temperature (873.15–1273.15 K), pressure (220–260 bar), biomass feed (18–69%), and gasifying agents on hydrogen and methane formation were analyzed. Higher temperatures and biomass feed percentages favored hydrogen production, while lower temperatures increased methane formation. At 1273.15 K, RDF showed the highest hydrogen yield in SCWG, rising from 0.43 to 1.42 mol, followed by Energy Sugarcane (0.39 to 1.23 mol), Coffee Husk (0.34 to 0.74 mol), and Eucalyptus Biochar (0.33 to 0.62 mol). In CO_2 gasification, hydrogen yields were lower but followed a similar trend. At 873.15 K, RDF also exhibited the highest methane increase in SCWG, from 0.14 to 0.91 mol, followed by Energy Sugarcane (0.12 to 0.65 mol), Coffee Husk (0.11 to 0.36 mol), and Eucalyptus Biochar (0.11 to 0.29 mol). Methane formation in CO_2 gasification was significantly lower, with RDF increasing from 0.0035 to 0.35 mol, followed by Energy Sugarcane (0.0024 to 0.24 mol), Coffee Husk (0.0002 to 0.058 mol), and Eucalyptus Biochar (0.0002 to 0.028 mol). On the other hand, a slight increase in hydrogen formation was observed as pressure decreased, while the opposite effect was observed for methane formation, with a small increase in its production as pressure increased. The impact of pressure change on the equilibrium compositions was not as significant as the effect observed by varying temperature; this behavior was observed in both gasification processes studied. Additionally, the behavior of the H_2/CO molar ratio for each biomass in the studied gasification processes was analyzed to assess the potential uses of the produced syngas. It was observed that the SCWG resulted in significantly higher H_2/CO molar ratios compared to CO_2 gasification.

Keywords: biomass; supercritical water gasification; carbon dioxide gasification; hydrogen; methane

Academic Editors: George Z. Papageorgiou, Maria Founti and George N. Nikolaidis

Received: 14 December 2024
Revised: 7 January 2025
Accepted: 8 January 2025
Published: 10 January 2025

Citation: Caraballo, L.D.G.; dos Santos Junior, J.M.; Zelioli, I.A.M.; Castillo Santiago, Y.; Bayer, J.F.P.; Mariano, A.P. Thermodynamic Assessment of Different Feedstocks Gasification Using Supercritical Water and CO_2 for Hydrogen and Methane Production. *Eng* **2025**, *6*, 12. https://doi.org/10.3390/eng6010012

1. Introduction

The concern over the increasing negative environmental impact caused by anthropogenic activities, particularly CO_2 emissions into the atmosphere and soil pollution, has generated significant interest in recent years. These concerns, linked with the growing need for new sources of renewable energy due to the finite nature of fossil fuels, have sparked the interest of researchers in developing strategies focused on circular economy principles. These strategies aim to minimize waste generation, pollutants, and CO_2 emissions, while simultaneously producing higher value-added products [1].

Regarding the use of agro-industrial waste—specifically lignocellulosic materials such as sugarcane bagasse, Coffee Husk Biochar, and Eucalyptus Biochar—along with processed urban solid waste, particularly Refuse-Derived Fuel (RDF), for conversion into higher value-added products represents an interesting alternative, especially for regions where agro-industrial waste generation is high, such as in Brazil [2]. This also serves as a favorable strategy for urban solid waste management [3], particularly in areas facing environmental issues related to landfill collapses [4].

An effective strategy to harness these wastes, particularly their stored chemical energy within the framework of the circular economy, is through thermochemical processes such as gasification. In this process, biomass reacts with a gasifying medium (steam, air, or oxygen) under specific feedstock, temperature, and pressure conditions to produce gases and liquids of greater interest, such as hydrogen [5].

One of the known biomass gasification processes is the one that uses supercritical water as the gasifying medium (Supercritical Water Gasification, SCWG). In this process, water in supercritical conditions (temperatures above 374.29 °C and pressures greater than 22.089 MPa) reacts with biomass to produce syngas (which is primarily composed of CH_4, H_2, CO, and CO_2). Under these conditions, water changes its physicochemical properties: its solvent nature shifts from polar to non-polar due to a decrease in dielectric constant, and it shows improved solubility in solid organic compounds and light gaseous products. This results in faster reactions due to a reduced interfacial mass transfer barrier [5].

Another biomass gasification process involves the use of CO_2 as the gasifying agent. In this process, CO_2 serves a dual purpose: reducing atmospheric CO_2 levels while producing syngas. However, the primary challenge of this method lies in its need for a continuous external energy source to maintain the gasification temperature, known as allothermal gasification [6].

Biomass gasification is a complex process where multiple chemical reactions occur simultaneously [6]. There are four key chemical reactions for the processes mentioned above (see Table 1).

Table 1. Key chemical reaction in biomass gasification.

$C + CO_2 \leftrightarrow 2CO$	Endothermic;
$C + H_2O \leftrightarrow CO + H_2$	Endothermic;
$C + 2H_2 \leftrightarrow CH_4$	Exothermic;
$CO + H_2O \leftrightarrow CO_2 + H_2$	Exothermic.

In the work of Tang and Kitagawa [7], a thermodynamic model applying the Gibbs energy minimization technique in combination with the Peng–Robinson Equation of State (EoS) was developed to estimate the equilibrium compositions in a supercritical water gasification process of biomass derived from starch and sawdust. The calculations were limited to temperatures above 923 K and a 10 to 15% feedstock range. The estimations were in good agreement with experimental data and indicated that temperature and the initial biomass feed percentage to the system are key factors in this gasification process. The same

model was used to calculate the equilibrium compositions of hydrogen and methane for the supercritical water gasification process of methanol and glucose, where it was observed that the mole fraction of hydrogen increased with temperature, while the opposite effect was observed for methane. Khonde et al. [8] estimated equilibrium compositions for the steam catalytic gasification of municipal solid waste using the Gibbs energy minimization approach. The equilibrium compositions were estimated to be 600 to 900 °C, assuming both complete and incomplete carbon conversion. According to the results, it was observed that an increase in temperature led to a rise in hydrogen and carbon monoxide formation, while methane formation slightly decreased with the temperature increase. The developed model showed a better fit to the experimental data when incomplete carbon conversion was considered, with root mean square error (RMSE) values of 0.1651 and 0.1489 for hydrogen and methane, respectively.

In Moravvej et al.'s study [9], predicted product gas yields from the supercritical water gasification of various feedstocks, including glycerol, lignin, humic acid, and ethylene glycol, were estimated using the Gibbs energy minimization method with a non-stoichiometric approach. The effect of temperature and feedstock concentration in the feed stream was evaluated over 375 °C to 800 °C for temperature and 5% to 40%wt for feedstock concentration. The results indicated that hydrogen yield increased as temperature rose for all feedstocks analyzed except lignin, while the opposite trend was observed for methane formation. The effect of feedstock percentage in the feed stream was evaluated for glycerol and ethylene glycol, where it was observed that as the feedstock percentage increased, hydrogen yield decreased, and methane yield increased. Compared to experimental data, the developed model provided suitable estimates for polar feedstocks with linear chains, such as glycerol and ethylene glycol, with average absolute relative deviations (AARD) of 2.70% and 0.17%, respectively. However, the model failed to accurately predict the yields for feedstocks with aromatic structures and high molecular weight, such as lignin and humic acid, obtaining AARDs of 11.23% and 25.95%, respectively.

In this study, estimated equilibrium compositions in gasification processes of various agro-industrial residues (composed of Energy Sugarcane biomass, Coffee Husk Biochar, and Eucalyptus Biochar) as well as a Refuse-Derived Fuel (RDF), using supercritical water and carbon dioxide as gasifying agents, are studied to identify trends that would indicate the temperature, pressure, and %feedstock under which the highest hydrogen and methane production levels are achieved, using the TeS® v.2 (Thermodynamic Equilibrium Simulation) software developed by Mitoura and Mariano [10]. This software allows for the calculation of equilibrium compositions using thermodynamic models based on Gibbs free energy minimization and entropy maximization methods, combined with the use of the Peng–Robinson equation of state to represent the system's behavior, employing a non-stoichiometric approach (considering all possible reactions).

No parametric study of the equilibrium compositions of RDF compared to agro-industrial residues using a non-stoichiometric thermodynamic model was found in the reviewed literature, highlighting the novelty of this study.

2. Methodology

2.1. Experimental Assessment of Different Feedstocks

Among the analyses performed on the feedstocks evaluated herein, the elemental analysis provides fundamental information for the thermodynamic approach to the processes of interest. The elemental analysis results presented in Table 2 were obtained using the CHONS elemental analyzer, brand Elementar (Langenselbold, Germany), model Vario MACROCube, equipped with a thermal conductivity detector (TCD).

Table 2. Elemental analysis for verified feedstocks.

	C (%)	H (%)	O (%)	N (%)	S (%)	Supplier	Nationality
Energy Sugarcane biomass	48.97	7.48	42.92	0.36	0.27	Nussed	Brazil
Coffee Husk Biochar	62.86	3.93	30.90	2.11	0.20	NetZero	Brazil
Eucalyptus Biochar	67.21	2.80	28.81	0.89	0.29	Grama Cultivo Eficiente	Brazil
Waste-Derived Fuel	55.12	9.89	33.76	0.94	0.29	Corpus	Brazil

For sample preparation, the samples were placed in tin foil, molded into capsule shapes, and individually weighed with an approximate mass of 100 mg. The capsules were then pressed and submitted to the equipment for analysis. The methodology involved catalytic combustion, separating interfering gases, and isolating the components of interest for measurement. The operational conditions included specific temperatures for the different components of the equipment: 1150 °C in the combustion tube, 850 °C in the reduction tube, 240 °C in the CO_2 column, 150 °C in the H_2O column, and 230 °C in the SO_2 column.

The Energy Sugarcane sample showed significant carbon (48.97%) and oxygen contents (42.92%), with low nitrogen (0.36%) and sulfur (0.27%) levels, suggesting a low potential for the formation of nitrogenous and sulfurous compounds in bio-oil and syngas produced during pyrolysis and gasification processes, respectively. These results align with those reported by Cui et al. [11]. The Coffee Husk Biochar sample exhibited a high carbon content (62.86%) and reduced oxygen content (30.90%), reflecting the thermal degradation of hemicellulose and cellulose in the biomass during its production. The nitrogen content (2.11%) was higher than the other feedstocks, indicating the potential for nitrogenous compound formation in derived products. The Eucalyptus Biochar sample presented the highest carbon content (67.21%) and the lowest hydrogen content (2.80%), also demonstrating a significant reduction in oxygen (28.81%) due to its production under the thermochemical conversion process. Both biochar samples (Coffee Husk and Eucalyptus) exhibited low sulfur contents (0.20% and 0.29%, respectively), consistent with biochar produced through thermochemical processes. The Waste-Derived Fuel sample had a high carbon content (55.12%) and a notable hydrogen content (9.89%), attributed to the presence of plastics, which aligns with findings by Aluri et al. [12]. This substrate reflects the high degree of processing of municipal solid waste.

It is important to mention that an understanding of the energy recovery potential of the different biomasses analyzed can be obtained through the H/C and O/C atomic ratios, as the calorific value of the biomasses decreases as the H/C and O/C ratios increase [5]. Brotel et al. [13] evaluated the energy potential of five species of Eucalyptus compared to four different biomass species (Coconut Husk, Elephant Grass, Bamboo, and Sugarcane Bagasse) through the analysis of their chemical, physical, and energy properties. Among the results obtained, they found that the lowest Lower Heating Value (LHV) within the Eucalyptus species samples corresponded to the sample that presented the highest H/C and O/C ratios.

Among the biomasses analyzed in this study, RDF biomass presents the highest H/C ratio and the second-highest O/C ratio. Conversely, Eucalyptus Biochar has the lowest atomic ratios. This difference in H/C and O/C atomic ratios may inspire future studies on potential energy recovery applications using the analyzed biomasses.

2.2. Thermodynamic Approach to Equilibrium Calculations in Reaction Systems

To predict the biomass gasification process, the Gibbs energy minimization (minG) thermodynamic approach was utilized. A system reaches thermodynamic equilibrium when the total Gibbs free energy is minimized, which makes this objective function widely used to analyze processes under equilibrium conditions [14].

Although one of the limitations of this thermodynamic model is that the equilibrium condition is generally not achieved in a real gasifier (as an infinite reaction time would be required), and it cannot predict the influence of hydrodynamic and geometric parameters, such as fluidization velocity or design variables like gasifier height, its significant advantage lies in the fact that it does not require knowledge of reaction mechanisms to estimate equilibrium compositions. It is particularly well-suited for fuels whose chemical formula is unknown, such as biomass. Furthermore, it is useful for studying the influence of fuel and process parameters on equilibrium compositions and provides a reasonable prediction of the maximum achievable yields of the products of interest [5,15].

Furthermore, the Gibbs energy minimization method offers significant advantages due to its straightforward minimization approach, which effectively predicts phase formation and describes equilibrium compositions. Studies by Rocha and Guirardello [16], Voll et al. [17], and Hantoko et al. [18] highlight these benefits. This method also considers mass conservation and fugacity equilibrium alongside minimizing Gibbs's energy, eliminating the need to predict the system's potential phases beforehand [19].

In reactive systems with multiple components under constant pressure and temperature, the equilibrium condition can be defined as a Gibbs energy minimization problem, with Gibbs energy represented in Equation (1).

$$minG = \sum_{i=1}^{NC}\sum_{k=1}^{NF} n_i^k\left[\mu_i^o + RTln\left(\hat{f}_i^k\middle/ f_i^o\right)\right] \tag{1}$$

Direct minimization of Equation (1), while incorporating mass balance and stoichiometric constraints, leads to a state where both chemical and phase equilibria are achieved. To ensure an appropriate solution, two additional restrictions must be applied.

The first constraint enforces the non-negativity of the mole quantities, as given in Equation (2), for each component across all phases [19]. The second one addresses atomic balance. Due to the non-stoichiometric nature of the formulation, which does not account for specific reactions during the optimization, the optimal atomic arrangement is represented in Equation (3).

$$n_i^k \geq 0 \tag{2}$$

$$\sum_{i=1}^{NC}\sum_{i=1}^{NF} a_{mi}\left(n_i^k\right) = \sum_{j=1}^{NC} a_{mi}\left(n_i^0\right) \tag{3}$$

When the mass conservation equation is fulfilled, the Gibbs free energy reaches its minimum value as a multi-component system attains chemical equilibrium [20].

Considering that gasification processes in supercritical media occur under high pressure and temperature, no liquid-phase components are expected to form. Nevertheless, both phases will still be included in the modeling process. Equation (1) can then be reformulated regarding the chemical potentials and molar quantities of components in the solid, liquid, and vapor phases, as shown in Equation (4).

$$min\ G = \sum_{i=1}^{NC}\left(n_i^s\mu_i^s + n_i^v\mu_i^v + n_i^l\mu_i^l\right) \tag{4}$$

The standard chemical potential can be determined using Equations (5) and (6), which provides essential values for calculating the Gibbs energy by Equation (4).

$$\frac{\partial}{\partial T}\left(\frac{\mu_i^k}{RT}\right)_P = -\frac{\overline{H}_i^g}{RT^2} \tag{5}$$

$$\left(\frac{\partial \overline{H}_i^g}{\partial T}\right)_P = Cp_i^g \quad (6)$$

To simplify the thermodynamic modeling of the process, the solid phase will be treated as ideal (Equation (7)), eliminating the need to account for non-idealities. This hypothesis is reasonable given that, during gasification with supercritical water, large amounts of water are introduced into the reaction system, which inhibits the formation of solid phase components [19,21,22].

$$\mu_i^s = \mu_i^0 \quad (7)$$

In contrast to the assumption of ideality for the solid phase, the vapor and liquid phases cannot be regarded as ideal due to the process conditions preventing this simplification.

Table 3 presents the parameters for calculating the components' saturation pressures and formation properties. Table 4 provides the parameters needed to calculate the heat capacities of the vapor phase components, and Table 5 lists the parameters for calculating the heat capacities of the solid phase components. The reference state for a species in the gas phase is defined as the pure substance at 1 bar and the system temperature, while for liquids and solids, it is the pure liquid or solid at 1 bar [23].

Table 3. Critical properties, formation, and parameters of the Antoine equation reported by Poling et al. [24].

Components	T_c (K)	P_c (bar)	V_c (m^3/kmol)	ω	a *	b *	c *	ΔH_f (cal/mol)	ΔG_f (cal/mol)
H_2O	647.140	220.640	0.056	0.344	18.304	3816.440	−46.130	-5.78×10^4	-5.46×10^4
H_2	32.980	12.930	0.064	−0.217	13.633	164.900	3.190	0.00×10^0	0.00×10^0
CH_4	190.560	45.990	0.099	0.011	15.224	597.840	−7.160	-1.78×10^4	-1.21×10^4
CO_2	304.150	73.740	0.094	0.225	22.590	3103.390	−0.160	-9.41×10^4	-9.43×10^4
CO	132.850	34.940	0.093	0.045	14.369	530.220	−13.150	-2.64×10^4	-3.28×10^4
O_2	154.580	50.430	0.073	0.022	15.408	734.550	−6.450	0.00×10^0	0.00×10^0
N_2	126.200	33.980	0.090	0.037	14.954	588.720	−6.600	0.00×10^0	0.00×10^0
CH_4O	512.640	80.970	0.118	0.565	18.588	3626.550	−34.290	-4.80×10^4	-3.88×10^4
C_2H_6	305.320	48.720	0.146	0.099	15.664	1511.420	−17.160	-2.00×10^4	-7.61×10^3
C_3H_8	369.830	42.480	0.200	0.152	15.726	1872.460	−25.160	-2.50×10^4	-5.81×10^3
NH_3	405.400	113.530	0.072	0.257	16.948	2132.500	−32.981	-1.10×10^4	-3.92×10^3
C_2H_4	282.340	50.410	0.131	0.087	15.534	1347.010	−18.150	1.25×10^4	1.64×10^4

* To calculate saturation pressure, the following equation was used: $\ln P_i^{sat} = a_i - \frac{b_i}{c_i + T}$.

Table 4. Coefficients for calculating the heat capacity of the formation of components in the vapor phase reported by Poling et al. [24].

Components	A_0 *	A_1 *	A_2 *	A_3 *	A_4 *
H_2O	87.329	-8.32×10^{-3}	2.79×10^{-5}	-3.11×10^{-8}	1.26×10^{-11}
H_2	57.285	7.31×10^{-3}	-1.53×10^{-5}	1.38×10^{-8}	-4.23×10^{-12}
CH_4	90.766	-1.78×10^{-2}	7.21×10^{-5}	-6.77×10^{-8}	2.17×10^{-11}
CO_2	64.756	2.69×10^{-3}	2.98×10^{-5}	-4.72×10^{-8}	2.10×10^{-11}
CO	77.731	7.78×10^{-3}	2.35×10^{-5}	-2.59×10^{-8}	1.02×10^{-11}
O_2	72.128	-3.56×10^{-3}	1.31×10^{-5}	-1.19×10^{-8}	3.56×10^{-12}
N_2	70.320	-5.19×10^{-4}	1.39×10^{-7}	3.12×10^{-9}	-1.97×10^{-12}
CH_4O	93.667	-1.39×10^{-2}	8.37×10^{-5}	-8.83×10^{-8}	3.05×10^{-11}
C_2H_6	83.017	-8.80×10^{-3}	1.12×10^{-4}	-1.32×10^{-7}	4.94×10^{-11}
C_3H_8	76.440	1.02×10^{-2}	1.19×10^{-4}	-1.57×10^{-7}	6.12×10^{-11}
NH_3	84.209	-8.38×10^{-3}	4.06×10^{-5}	-4.22×10^{-8}	1.51×10^{-11}
C_2H_4	83.880	-1.75×10^{-2}	1.15×10^{-4}	-1.34×10^{-7}	4.99×10^{-11}

* Values already multiplied by the gas constant (R = 1.987 cal/mol.K). To calculate Cp, the following polynomial was used: $Cp = A_o^i + A_1^i T + A_2^i T^2 + A_3^i T^3 + A_4^i T^4$.

Table 5. Coefficients for calculating the heat capacity of solid formation reported by Smith et al. [25].

Components	*A* *	*B* *	*C* *
C	35.190	1.53×10^{-3}	-1.72×10^{5}

* Values already multiplied by the gas constant (R = 1.987 cal/mol.K). To calculate Cp, the following polynomial was used: $Cp = A^i + B^iT + C^iT^2 + D^iT^{-2}$.

Estimation of Fugacity Coefficients Using the Cubic Peng–Robinson Equation

The Gibbs energy minimization (minG) thermodynamic approach was employed to predict the biomass gasification process from a phenomenological perspective. A system reaches thermodynamic equilibrium when the total Gibbs free energy is minimized, making this objective function widely used to evaluate processes in equilibrium conditions [14]. This methodology offers significant advantages, as it directly minimizes the Gibbs energy to predict phase formation and effectively describes equilibrium compositions in reaction systems.

The equations of state can be represented as cubic equations, expressed in terms of the compressibility factor *Z*, typically formulated as shown in Equation (8).

$$f(Z) = Z^3 - (1 + B - uB)Z^2 + \left(A + wB^2 - uB - uB^2\right)Z - AB - wB^2 - wB^3 \quad (8)$$

where A and B are dimensionless variables that depend on temperature, pressure, and phase composition, as defined in Equations (9) and (10). The parameters u and w, with values of 2 and -1, respectively, are constants provided by the Peng–Robinson equation of state.

$$A = \frac{a_m P}{(RT)^2} \quad (9)$$

$$B = \frac{b_m P}{RT} \quad (10)$$

In this context, a_m and b_m represent the mixture properties determined by using Equations (11) and (12), respectively.

$$a_m = \sum_{i=1}^{NC}\sum_{j=1}^{NF} y_i y_j \sqrt{a_i a_j}\left(1 - k_{ij}\right) \quad (11)$$

$$b_m = \sum_{i=1}^{NC} y_i b_i \quad (12)$$

k_{ij} is a binary interaction parameter, while ai and a_j are parameters that depend on predetermined constants specific to each equation of state, including the critical properties (pressure P and temperature T), the gas constant R, and the acentric factor ω_i for each component i and j. Thus, a_i and a_j are expressed as shown in Equation (13).

$$a_i = 0.45724 \frac{R^2 {T_{c,i}}^2}{P_{c,i}} \alpha_i \quad (13)$$

The parameter α_i is given by Equation (14).

$$\alpha_i = \left[1 + \left(0.37464 + 1.54226\omega_i - 0.26992\omega_i^2\right)\left(1 - \sqrt{\frac{T}{T_{c,i}}}\right)\right]^2 \quad (14)$$

The b_i parameter also depends on the critical properties, gas constant, and acentric factor of each component i, as shown in Equation (15).

$$b_i = 0.07780 \frac{RT_{c,i}}{P_{c,i}} \tag{15}$$

With these data, it becomes possible to compute the roots of the cubic equation. The presence of a single real root of the compressibility factor indicates that the mixture exists in one phase, either liquid or vapor. If there are three real roots, the largest will correspond to the vapor phase, while the smallest will represent the liquid phase. The intermediate root has no physical significance as it violates the mechanical stability criterion [26]. Once the root of Equation (8) is determined for both phases, Equation (16) is utilized to estimate the fugacity coefficients for the vapor and liquid phases.

$$\ln \hat{\varnothing}_i = \frac{B_i}{B}(Z-1) - \ln(Z-B) + \frac{A}{2\sqrt{2}B}\left(\frac{B_i}{B} - 2\frac{\sum_j y_i \sqrt{a_i a_j}}{a_m}\right) ln\left(\frac{z + \left(1+\sqrt{2}\right)B)}{z + \left(1-\sqrt{2}\right)B}\right) \tag{16}$$

2.3. Mathematical Formulation and Equilibrium Calculations

Initially, 12 components were considered (H_2, H_2O, CH_4, CO_2, CO, O_2, N_2, CH_4O, C_2H_6, C_3H_8, NH_3, C_2H_4) as representative of the primary compounds that can form during the reaction processes verified in this study. The selection of these components is grounded in literature findings, which indicate that these species are typically produced in significant quantities during biomass gasification from various biomass sources [7,19,21,22,27–32].

The formulated nonlinear programming (NLP) problems were addressed using the TeS—Thermodynamic Equilibrium Simulation v2 software, implemented in Python, and the IPOPT solver available in the Pyomo framework. Python was chosen due to its versatility and the extensive range of libraries available for scientific computing, making it ideal for developing robust thermodynamic models. The use of IPOPT, specifically within Pyomo, is motivated by its robustness and efficiency in handling highly nonlinear models typical of Gibbs energy minimization calculations, which are essential for predicting chemical reactions.

Figure 1 presents a simplified schematic of the information processing flow in the TeS v2 simulator. This simulator adopts Gibbs energy minimization as its primary criterion. Initially, it is necessary to specify the compositions of the initial components in the reaction system, along with their thermodynamic properties, temperature, and pressure. The atomic balance is then expanded, creating an equation for each component. Consequently, the optimization problem is subject to n + 1 constraints: n for the possible components in the reaction system and one for the non-negativity of the number of moles. Each component is considered unique in both phases, resulting in three groups of variables, one for each phase.

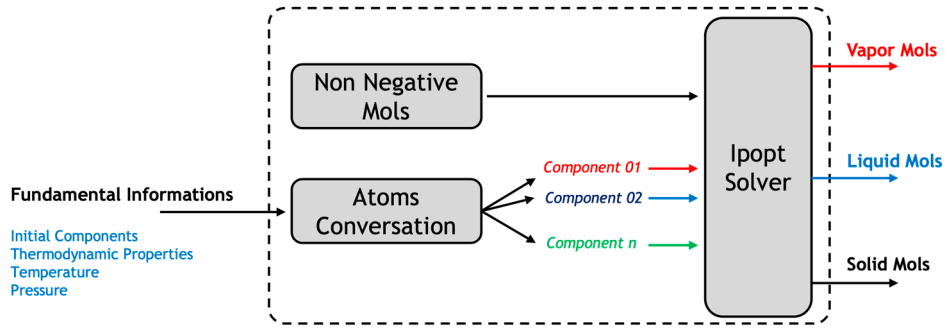

Figure 1. Simplified schematic of the TeS simulator.

IPOPT is particularly advantageous in this context because it can solve large-scale, nonlinear optimization problems with high precision. It employs an interior-point algorithm optimized for sparse matrices, which aligns well with chemical equilibrium systems' complex and multidimensional nature. The open-source nature of both Python and IPOPT allows for fine-tuning of solver parameters, enabling enhanced control over convergence criteria and solution accuracy, both crucial for achieving reliable results in mixed-phase and multiphase systems. This Python-based approach has consistently demonstrated high levels of accuracy and efficiency, producing excellent results in various chemical equilibrium scenarios similar to approaches highlighted in various literature [7,29,31,32].

3. Results and Discussions

3.1. Methodology Validation

As a fundamental step in the use of computational methodologies for process prediction, this section presents a discussion on the validation of the methodology employed in this work using the TeS v2.0 software with the IPOPT solver to solve Gibbs energy minimization problems for equilibrium calculations.

Figure 2 presents a comparison between the data reported by Tang and Kitagawa [7] for the Supercritical Water Gasification (SCWG) of methanol and the results calculated using the methodology described in this study. It is important to highlight that the data provided by Tang and Kitagawa are simulated, considering an SCWG process at 276 bar, with methanol feed fixed at 15%wt. For these results, both phases were treated as ideal, resulting in an excellent fit with the data presented by the authors.

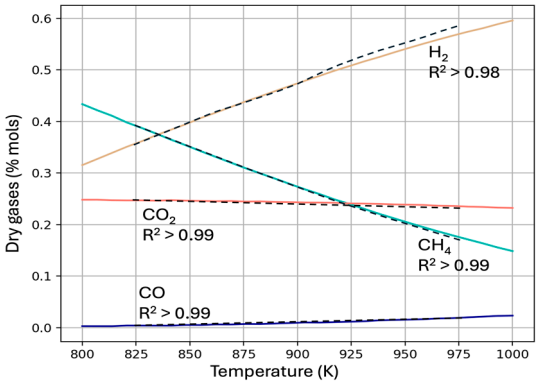

Figure 2. Validation of the methodology with data reported by Tang and Kitagawa [7] for the supercritical water gasification of methanol at 276 bar with a feed concentration of 15%wt methanol (dashed lines: Tang and Kitagawa [7]; solid-colored lines: this work).

Figure 2 shows the compositions of the dry gas stream as a function of the reactor temperature. For both components, an excellent fit is observed, with determination coefficients above 0.98. Considering that the SCWG process for methanol shares a similar complexity with the processes discussed in this study, the excellent fit of Tang and Kitagawa's data with the results obtained through the TeS v2.0 software supports the applicability of this methodology for analyzing other SCWG processes, including those involving biomass, as discussed in this work.

Additionally, another validation test was developed using data reported by Freitas and Guirardello [19]. The authors investigated the effect of CO_2 addition on the behavior of the SCWG process for sugarcane bagasse biomass. For this study, the composition of the biomass used was obtained from results reported by Osada et al. [33], as can be seen in Table 6.

Table 6. Composition of sugarcane bagasse biomass.

w *	x *	y *	z *
3.69	6.00	3.08	0.028

* Equation: $C_wH_xO_yN_z$.

In order to simulate the process under the same conditions presented by the authors, the pressure will be fixed at 260 bar, the temperature of the reaction system will be varied between 973.15 and 1173.15 K, the biomass composition will be fixed at 15%wt, and CO_2 additions will be set at values of 0 and 15%wt. Figure 3 presents the comparison of the results obtained by applying the methodology described in this paper concerning the data reported by Freitas and Guirardello [19].

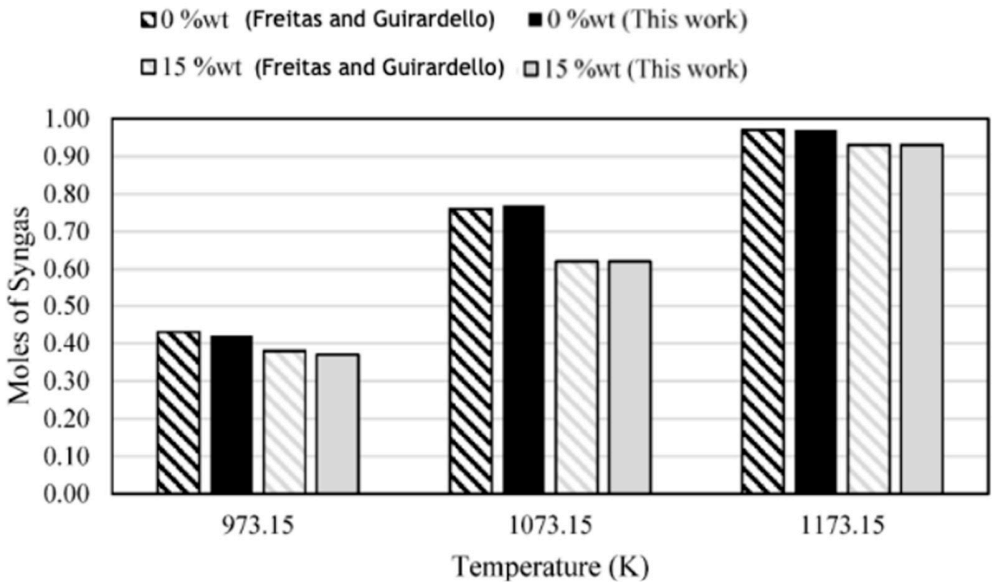

Figure 3. Comparison between simulated data and data reported by Freitas and Guirardello [19] for the SCWG process of sugarcane bagasse biomass with CO_2 addition.

The results presented in Figure 3 show an excellent fit between the simulated data and the results reported by Freitas and Guirardello [19], with a determination coefficient (R^2) greater than 0.99. This performance reinforces the reliability of the methodology described in this study for simulating complex reactions involving supercritical water and carbon dioxide under extreme temperature and pressure conditions.

3.2. Study of Hydrogen and Methane Equilibrium Compositions of SCW and CO_2 Gasification of Different Feedstock Types

3.2.1. Supercritical Water Gasification (SCWG)/CO_2 Gasification

The analysis of the equilibrium compositions in the gasification processes with supercritical water and CO_2 was conducted under defined and controlled temperature and pressure conditions. The temperature varied from 873.15 to 1273.15 K (which is approximately within the typical range of a gasification process [34]), and the pressure was from 220 to 260 bar (selected considering the pressure required for gasification with supercritical water). The % biomass fed to the system ranged from 18% to 69% (on a molar basis), with a constant amount of water or CO_2 of 1.11 mol.

In Figure 4, the main products from the gasification processes with SCW and CO_2 for the different feedstock types can be observed. In these reactions, other products were also formed in minimal amounts ($<7 \times 10^{-3}$ mol) for all verified feed conditions, such as NH_3, N_2, CH_3OH, C_2H_6, and C_4H_{10}. However, these compounds' concentration (molar

fraction) is lower than that of the main products and has a minimal impact on their formation reactions, although some biomass obtained from farming and food production could contain relative concentration levels of nitrogen and sulfur [35,36]. It is important to mention that the presence of ammonia in the syngas can lead to catalyst poisoning effects when specific limits are reached (depending on the catalyst used) and affect the performance of reactors in downstream applications, such as the production of transportation fuels from biomass through Fischer–Tropsch synthesis [37]. Likewise, high nitrogen concentrations could result in a dilution effect of the syngas reactive gases, reducing the efficiency of subsequent processes. This situation commonly occurs when air is used as the gasifying medium. Furthermore, in Figure 4, the synergistic effect of temperature and the biomass feed ratio on the main target products can be observed. In general, it can be seen that for both supercritical water and CO_2 gasification, the increase in temperature and biomass feed ratio promotes the production of hydrogen and carbon monoxide for all biomasses analyzed. For instance, in the case of hydrogen production from RDF in SCWG at 220 bar, we observed an increase from approximately 0.07 mol with 18% biomass fed into the system at a temperature of 873.15 K, up to 0.44 mol when the temperature was raised to 1273.15 K, maintaining a constant % biomass fed to the system. Furthermore, by increasing the % biomass fed to the system to 69% at a temperature of 1273.15 K, hydrogen production reached values of 1.42 mol. This trend is also observed in carbon monoxide formation for all biomass types analyzed, highlighting the influence of both temperature and biomass composition on the formation of these two key products. This can be attributed to the fact that the reactions for forming these compounds (H_2 and CO) are endothermic and, therefore, favored by the exothermic nature of the gasification processes. This condition is particularly interesting when attempting to produce the maximum possible amount of hydrogen [38].

On the other hand, this increase in temperature has the opposite effect on methane production, which can be attributed to the fact that the reactions for methane formation are exothermic and, therefore, not favored by the increase in temperature [5].

It can be observed that supercritical water gasification presents higher levels of methane formation compared to CO_2 gasification, which can be ascribed to the fact that the SCWG process produces higher levels of H_2 and CO, components necessary for methane formation through the reaction $2CO + 2H_2 \leftrightarrow CH_4 + CO_2$.

The trend observed in the production of hydrogen and methane with the increase in temperature has also been evidenced in other related studies:

Chutichai et al. [39] investigated the steam gasification of Japan cedar biomass in a circulating fluidized bed reactor using the Aspen Plus simulator. The gasifier temperature varied from 500 to 1000 °C, and it was observed that the hydrogen composition in the product gas increased significantly as the gasifier temperature rose, reaching a level of 61% H_2 at approximately 700 °C, while the opposite effect was observed for the methane composition.

Lu et al. [40] analyzed the equilibrium compositions obtained in the supercritical water gasification of Wood sawdust biomass using a thermodynamic chemical equilibrium model. The temperature effect was studied from 673 K to 1073 K, at 25 MPa and a 5% dry biomass content. It was observed that the hydrogen yield increased with the temperature rise, reaching a maximum value of 88.623 mol/kg of dry biomass, while the methane yield decreased significantly.

Pinto et al. [41] analyzed the effect of temperature increase on the gas composition in the co-gasification of different mixing percentages of Wood pine residue with polyethylene (PE) using steam as the gasifying agent. The temperature range analyzed was from 730 to 900 °C, with the different mixing percentages of PE being 0%, 10%, and 40% (w/w),

and the steam-to-residue ratio was 0.8 (w/w). It was observed that the hydrogen yield increased significantly with the temperature rise, with increases of up to 100% for the mixture with 10% PE and 65% for the biomass with 40% PE. The opposite effect was observed for methane, with yields decreasing as temperature increased.

Sadhwani et al. [6] investigated the effect of temperature on the composition of the syngas produced from the gasification of Southern pine biomass using CO_2 as the oxidizing agent in a bench-scale atmospheric bubbling fluidized bed gasifier. The analysis was carried out over a temperature range from 700 to 934 °C. In the steady-state syngas composition profile versus temperature, it was observed that the hydrogen composition increased with temperature, while for methane, a decrease in composition was noticeable starting from 850 °C.

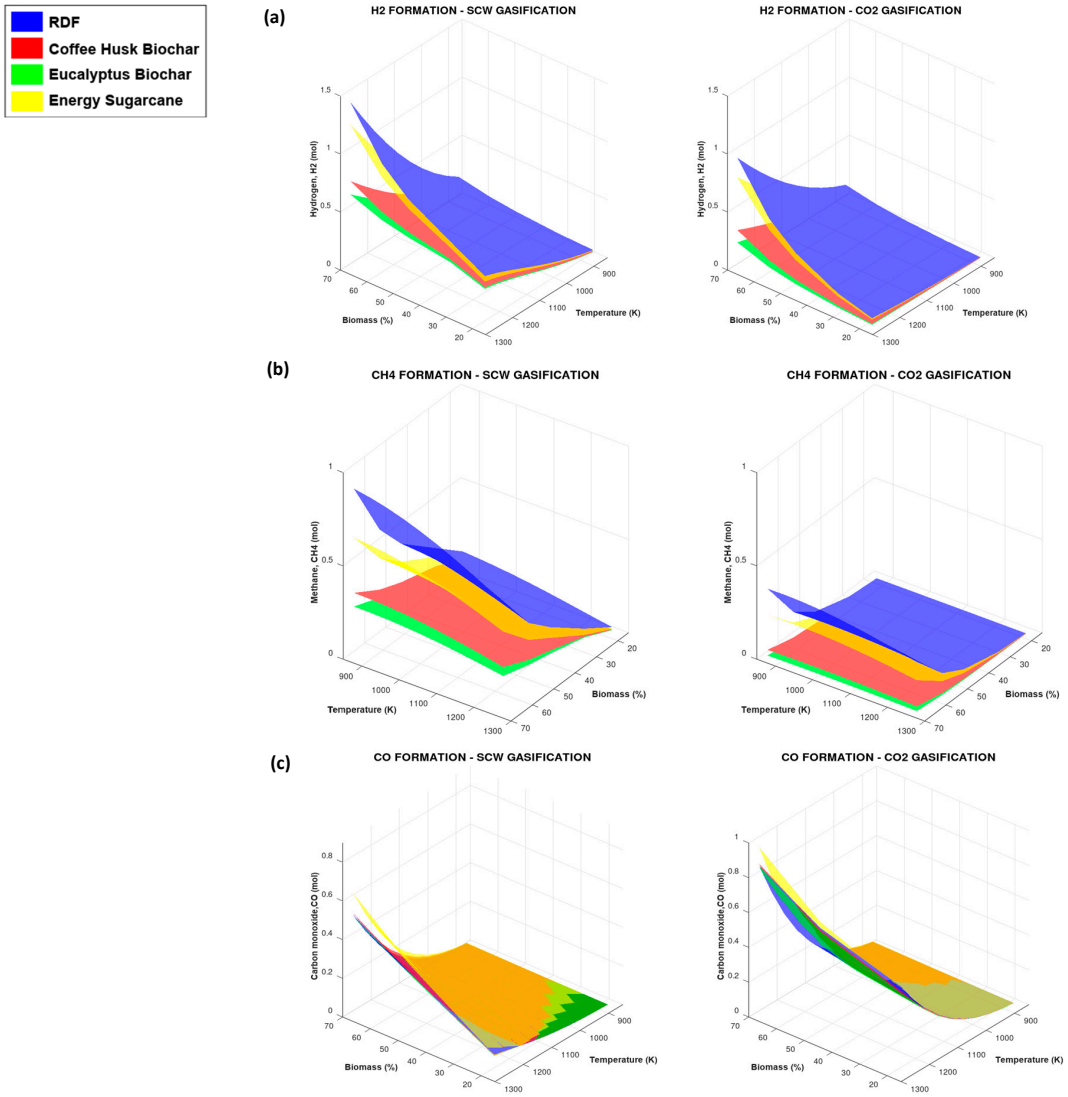

Figure 4. Equilibrium compositions of (**a**) hydrogen, (**b**) methane, and (**c**) carbon monoxide as a function of temperature and biomass composition in the process feed at 220 bar.

Analyzing the results for hydrogen formation in both gasification processes, it can be observed that, under the same conditions of temperature, pressure, and biomass composition, the supercritical water gasification (SCWG) process achieved higher levels of hydrogen production. For instance, in the case of Energy Sugarcane biomass, at a temperature of 1273.15 K, a pressure of 220 bar, and a % biomass fed to the system of 69%, the SCWG process produced 1.23 mol of H_2; meanwhile, 0.77 mol of H_2 was achieved with CO_2

gasification process, representing a difference of approximately 37%. This behavior was similar across all the biomass types analyzed. The increase in hydrogen production with the SCGW process compared to CO_2 gasification may indicate that part of the hydrogen produced also comes from water, confirming the fact that water in this type of process (SCW gasification) acts both as a reactant and as a reaction medium [42].

The RDF was the feedstock with the highest methane and hydrogen formation for both gasification processes (SCWG and CO_2G), followed by the biomasses Energy Sugarcane, Coffee Husk Biochar, and Eucalyptus Biochar, respectively. This can be attributed to the fact that RDF has the highest H/C ratio (2.14), meaning a greater number of hydrogen atoms per carbon atom, which was expected to result in higher levels of CH_4 and H_2 formation.

Regarding the formation of carbon monoxide, the Energy Sugarcane biomass exhibited the highest levels of formation, although the difference compared to the other biomasses was minimal. For instance, in the CO_2 gasification process at 220 bar, 1273.15 K, and a biomass composition of 69%, the Energy Sugarcane biomass produced 0.96 mol of CO, followed by 0.86, 0.85, and 0.85 mol of CO for Coffee Husk Biochar, Eucalyptus Biochar, and RDF, respectively. This trend is similar for the SCWG process. This can be attributed to the fact that the Energy Sugarcane biomass has the highest O/C ratio (0.66) compared to the other biomasses.

Besides analyzing the combined effect of temperature and the amount of biomass fed into the system, it is also essential to observe the effect of pressure variation on the equilibrium compositions of the target products. For this analysis, the biomass percentage in the feedstock was kept constant at 47%, the temperature varied within the range of 873.15 K to 1273.15 K, and the pressure ranged from 220 to 260 bar.

Figure 5 shows that the RDF exhibits the highest levels of hydrogen and methane formation, a behavior similar to that observed in Figure 4.

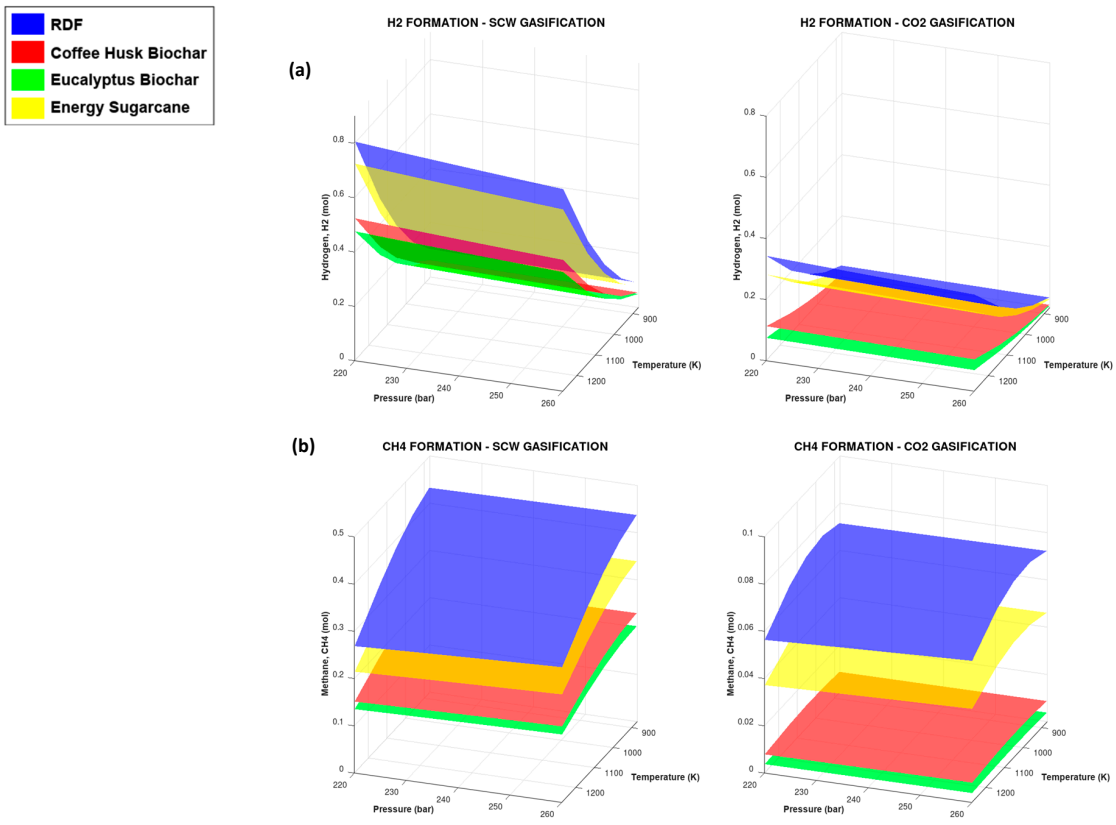

Figure 5. Equilibrium compositions of (**a**) hydrogen and (**b**) methane as a function of temperature and pressure at 47% of biomass in the process feed.

Based on the results obtained, it can be observed that an increase in pressure leads to a decrease in hydrogen formation while promoting an increase in methane, which is consistent with Le Chatelier's principle according to the following methane reaction $CH_4 + H_2O \leftrightarrow CO + 3H_2$. A similar result was obtained by Kitzler et al. [43] when varying temperature and pressure conditions in woody biomass gasification in a bubbling pressurized gasification plant.

3.2.2. Supercritical Water + CO_2 Gasification

To assess the impact of the simultaneous feeding of the two gasifying agents (supercritical water and CO_2) on the target reaction products, four feeding conditions were evaluated, with the pressure fixed at 220 bar. Table 7 presents the four selected conditions for the analysis.

Table 7. Initial moles (feed) for each condition.

	Condition 1	Condition 2	Condition 3	Condition 4
Pressure	220 bar	220 bar	220 bar	220 bar
Biomass initial mol	0.25	0.25	0.25	0.25
SCW initial mol	0.277	2.5	2.5	0.277
CO_2 initial mol	0.277	2.5	0.277	2.5

In Figure 6, it can be observed that the highest methane production under simultaneous feeding conditions of supercritical water and carbon dioxide occurs at temperatures between 873 and 1000 K in feeding condition number 3—that is, feeding a higher amount of water relative to the other reactants (biomass and CO_2). The Refuse-Derived Fuel (RDF) showed the highest levels of methane formation under all feeding conditions, which can be attributed to the fact that RDF has the highest H/C ratio.

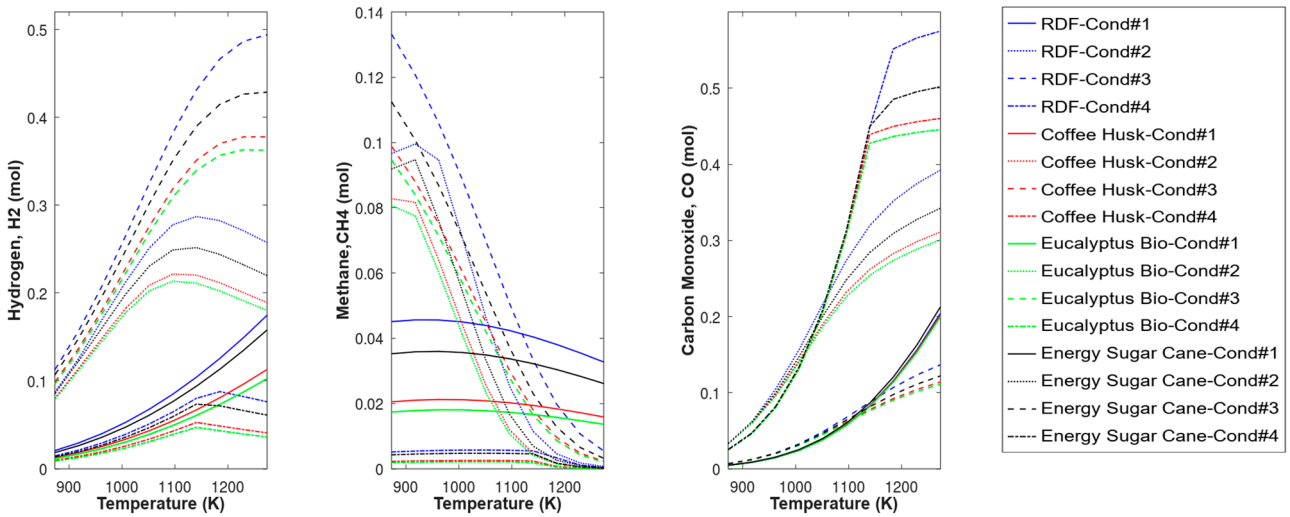

Figure 6. Hydrogen, methane, and carbon monoxide formation at 220 bar, with different feed conditions and temperature for SCWG + CO_2 Gasification.

It is also observed that there is an inverse relationship between temperature increment and methane production. At high temperatures, methane production decreases significantly for all feeding conditions, mainly due to the exothermic nature of the methane formation reaction, which is not favored by the increase in temperature [5].

Figure 6 also shows that the highest levels of hydrogen production are achieved by increasing the temperature in feeding condition 3, with a higher amount of water fed

relative to the other reactants. This is because the supercritical water gasification reaction is favored. The feedstock that produced the highest levels of hydrogen was Refuse-Derived Fuel (RDF), followed by Energy Sugarcane, Coffee Husk Biochar, and Eucalyptus Biochar, respectively. This can be ascribed to the fact that RDF has the highest H/C ratio.

It is also observed that for condition 2 (where higher amounts of water and CO_2 are fed simultaneously into the system relative to the amount of fuel), there is a gradual increase in hydrogen production as the temperature rises. However, around 1123 K, a marked decrease in hydrogen levels begins to be observed. This situation is also seen for condition 4, but it does not occur for feeding condition 1, where it is possible to observe that the levels of hydrogen produced increase gradually as the temperature rises.

The decrease in hydrogen production from approximately 1123 K for conditions 2 and 4 may be attributed to the exothermic nature of the Shift reaction ($CO + H_2O \leftrightarrow CO_2 + H_2$), which proceeds in the reverse direction, i.e., towards the production of CO and H_2O, thereby consuming CO_2 and H_2. In condition 1, lower amounts of CO_2 and H_2O moles are fed into the system. The reduction in CO_2 feed seems to influence hydrogen consumption. It can be inferred that with fewer CO_2 moles available for the reverse Shift reaction, a smaller amount of hydrogen moles is consumed. This hydrogen availability (due to no consumption in the reverse Shift reaction) is particularly evident in condition 1, especially at higher temperatures.

For all conditions, it was observed that Refuse-Derived Fuel (RDF) produced the highest levels of hydrogen and methane.

Similarly, in Figure 6, it is noticeable that the highest carbon monoxide production for all the biomasses occurs at higher temperatures and, specifically in condition 4, with a higher amount of CO_2 fed relative to the other reactants. This result agrees with the Boudouard reaction, which is endothermic ($C + CO_2 \leftrightarrow 2CO$). The RDF exhibited the highest levels of CO production among the other biomasses.

It is also observed that the increase in CO production follows an exponential behavior for condition 4 from 973 K to approximately 1173 K, after which the CO formation becomes less pronounced. This might suggest that, under these conditions of high temperature and equilibrium, other endothermic reactions could be favored.

3.2.3. Impact of Impurities and Heterogeneity in Biomass Feedstock

Only the presence of mineral components was considered for the impact of impurities on predicted compositions. In this study, a pseudocomponent composed of silica (SiO_2), metal oxides (Al_2O_3, Fe_2O_3, and MgO), calcium carbonate ($CaCO_3$), and calcium oxide (CaO) was introduced. These constituents are commonly found in residues due to the absorption of soil minerals, fertilizer residues, or natural processes [44]. Table 8 presents the composition of the pseudocomponent used to represent impurities in the substrates under investigation.

Table 8. Composition of the pseudocomponent considered as an impurity.

Component	%wt
SiO_2	60
Al_2O_3	10
Fe_2O_3	5
MgO	5
$CaCO_3$	5
CaO	15
Total	100

Figure 7 presents the Spearman correlation matrices for the biomass gasification processes using supercritical water (Figure 7a) and carbon dioxide (Figure 7b). The conditions adopted to obtain the results shown in Figure 7 are described in Table 9.

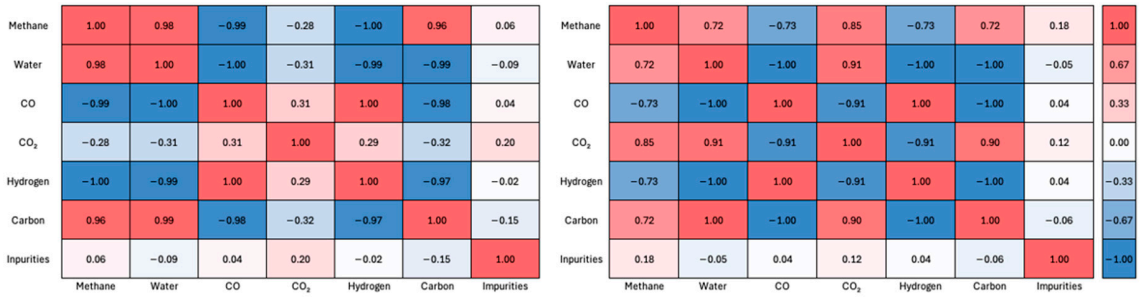

Figure 7. Spearman correlations to verify the effect of adding impurities on the formation of other components ((**a**): SCWG; (**b**): gasification with CO_2).

Table 9. Simulated conditions for verifying the effect of impurities on the behavior of the reaction process.

	Minimum	Maximum
Pressure (bar)	200	300
Temperature (K)	873.15	1273.15
Impurities (mols)	0.1	0.2
Water (mols)	0	1
Carbon Dioxide (mols)	0	1
Substrate (mols)	1	

The study of the influence of substrate impurities on the behavior of complex reaction processes, such as those examined in this paper, is challenging, considering that the applied thermodynamic approach is highly dependent on the availability of thermodynamic data for potential byproducts and impurities. Figure 7 illustrates the effects of impurity presence on component formation, focusing solely on processes using Energy Sugarcane biomass as the substrate and a pseudocomponent as a potential impurity, following the compositions presented in Table 7.

As shown in Figure 7, adding impurities has minimal influence on hydrogen formation but has a significant positive effect on carbon dioxide formation. This is expected, considering that both components involved in forming of the pseudocomponents contain the oxygen atom. Another interesting observation is that the presence of impurities tends to reduce the formation of solid carbon. However, the impurities are minimally consumed throughout the reaction processes, maintaining nearly constant concentrations during the processes under the conditions tested. This also prevents the formation of undesired components that could compromise the integrity of the processes during the progression of the reactions.

Figure 7 presents the results considering Energy Sugarcane biomass as the substrate. However, the observed behaviors are similar for the other substrates considered in this study.

To assess the effect that biomass heterogeneity in the feedstock could have on the equilibrium compositions in gasification with supercritical water and carbon dioxide, RDF biomass was selected as the reference for the comparison. The evaluation was conducted under pressure and temperature conditions of 220 bar and 1273.15 K, respectively. Three feed conditions were chosen for the analysis, which are described in Table 10.

Table 10. Feedstock composition for each condition evaluated.

Feedstock	Condition 1 (mol)	Condition 2 (mol)	Condition 3 (mol)
RDF	0.1 (10%)	0.4 (40%)	0.8 (80%)
Coffee Husk Biochar	0.4 (40%)	0.1 (10%)	0.05 (5%)
Eucalyptus Biochar	0.4 (40%)	0.1 (10%)	0.05 (5%)
Energy Sugarcane	0.1 (10%)	0.4 (40%)	0.1 (10%)

For all conditions, a total feed of 1 mol of Feedstock (38%) and 1.66 mol of gasifying agent (62%) was chosen.

Condition 1 represents a feedstock with a higher proportion of Coffee Husk Biochar and Eucalyptus Biochar, which have the lowest H/C ratios. Condition 2, on the other hand, aims to demonstrate the effect of increasing the proportion of biomasses with the highest H/C ratios (RDF and Energy Sugarcane). Finally, Condition 3 represents a feedstock primarily composed of the material with the highest H/C ratio—in this case, RDF.

All conditions were compared to the equilibrium composition for a homogeneous feed of 38% RDF and 62% gasifying agent, as this feedstock produced the highest hydrogen and methane production levels.

Figure 8 illustrates the effect of increasing the proportion of biomasses with a higher H/C ratio in the feed on the equilibrium compositions of H_2 and CH_4 for the two gasification processes studied. As expected, an increase in the proportion of RDF in the mixture enhances the production of these target compounds, reaching levels similar to the 100% RDF feed. The difference in hydrogen and methane production between the two gasification processes can be observed again.

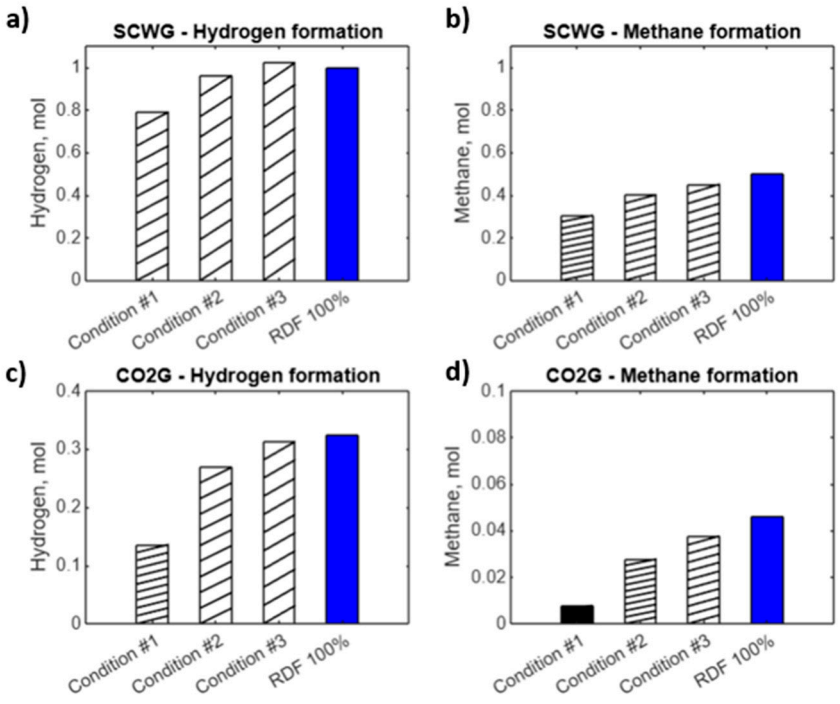

Figure 8. Moles of hydrogen and methane produced in co-gasification processes with supercritical water (SCWG) and carbon dioxide (CO_2G) at 220 bar and 1273.15 K.

3.2.4. H_2/CO Ratio Assessment

Gasification processes in supercritical water and carbon dioxide can be characterized by the production of syngas, which primarily consists of hydrogen and carbon monoxide.

In some cases, small amounts of carbon dioxide or methane are also present [5,45]. An important parameter for understanding the potential uses of the produced syngas is the H_2/CO molar ratio. When the H_2/CO molar ratio is approximately one, the formed syngas can be used to produce higher alcohols. For H_2/CO molar ratios close to two, methanol production is favored, which is an important intermediate for synthesizing various petrochemical products and fuels such as dimethyl ether (DME), gasoline, and biodiesel [46]. When the H_2/CO molar ratio is close to three, ammonia (NH_3) production is favored [10].

Figures 9 and 10 show the behavior of the H_2/CO molar ratio as a function of temperature and % biomass fed into the system for supercritical water and carbon dioxide gasification processes at 220 bar.

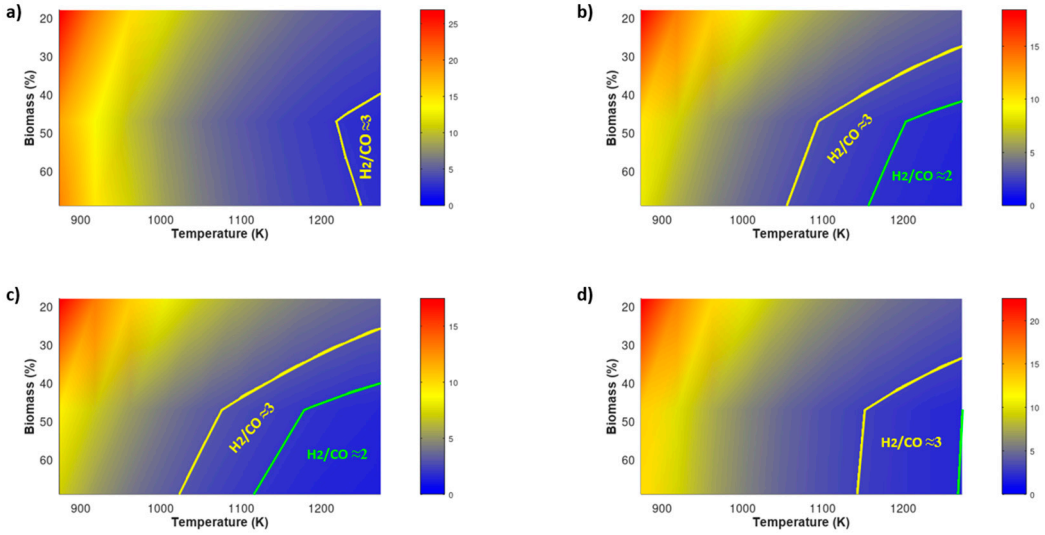

Figure 9. The H_2/CO molar ratio as a function of temperature and % biomass fed to the system for the SCW gasification process at 220 bar. (**a**) Refuse-Derived Fuel, (**b**) Coffee Husk, (**c**) Eucalyptus Biochar, (**d**) Energy Sugarcane.

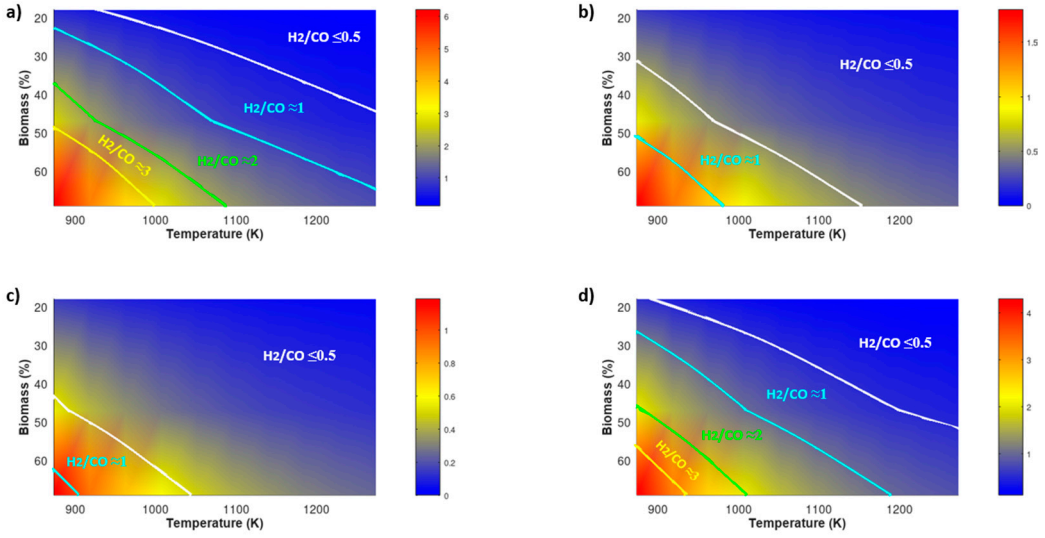

Figure 10. The H_2/CO molar ratio as a function of temperature and % biomass fed to the system for the CO_2 gasification process at 220 bar. (**a**) Refuse-Derived Fuel, (**b**) Coffee Husk, (**c**) Eucalyptus Biochar, (**d**) Energy Sugarcane.

Within the observed molar ratios of H_2/CO in Figures 9 and 10, ratios ≤ 1 were found, which indicates that the syngas may be suitable for ethanol production. Ratios of

approximately two were also observed, suggesting potential use for methanol production. Additionally, ratios ≥ 2 were found, appropriate for Fischer–Tropsch synthesis (light hydrocarbon production). Furthermore, much higher ratios were observed, which could warrant evaluation for potential applications in fields such as fertilizer and hydrogen fuel production [47].

Figures 9 and 10 also show a difference in the H_2/CO molar ratio behavior for the analyzed biomass in the gasification processes studied. Coffee Husk and Eucalyptus Biochar exhibited higher H_2/CO ratios, close to three, during supercritical water gasification, while for the carbon dioxide gasification process, RDF and Energy Sugar Cane biomasses showed similar values for the H_2/CO ratio in syngas formation. It can be observed that carbon dioxide gasification results in a higher amount of the H_2/CO molar ratio with values lower than 1. Thus, the Shift reaction ($CO + H_2O \rightarrow CO_2 + H_2$) is recommended to increase this ratio value [5]. Additionally, it is observed that supercritical water gasification results in higher hydrogen production levels compared to CO_2 gasification.

4. Conclusions

The equilibrium composition behavior for the gasification processes of agro-industrial waste and Refuse-Derived Fuel (RDF) with supercritical water and CO_2, as a function of variables such as temperature, pressure, and feedstock percentage, was found to be consistent with the expected results based on the reviewed literature. This provides evidence that support the applicability of the proposed methodology for evaluating the thermodynamic behavior of the processes mentioned above.

The composition of the biomass significantly influences the formation of hydrogen and methane. Higher H/C ratios result in increased levels of formation of these key products.

RDF exhibited the highest levels of hydrogen and methane formation, followed by Energy Sugarcane, Coffee Husk, and Eucalyptus Biochar biomass, respectively, due to RDF having the highest H/C ratio.

Similarly, temperature had a significant impact on the equilibrium compositions. Higher temperatures favored endothermic reactions, leading to higher hydrogen formation. In contrast, lower temperatures favored exothermic reactions, producing higher methane formation.

The gasification process with supercritical water produced the highest levels of formation of the target components (H_2 and CH_4) across all feedstock conditions. Gasification using both reactants, supercritical water and CO_2, simultaneously yielded higher hydrogen and methane formation levels when a higher amount of supercritical water was fed.

Based on the results, the operating parameters that provide the highest hydrogen formation levels are high temperature (1273.15 K), low pressure (220 bar), and the highest % biomass fed to the system (69%). Regarding methane formation, the parameters are low temperature (873.15 K), high pressure (260 bar), and the highest % biomass fed to the system (69%).

Finally, it is important to highlight that one of the potential limitations of the methodology employed is that, in real-world scenarios, equilibrium compositions are typically not attained. Additionally, this model type does not account for the effects of catalytic processes, mass transport phenomena, or reaction kinetics. Nevertheless, the estimations obtained provide a reasonable approximation and are useful for understanding qualitative data and trends in the studied gasification processes. Future research could employ this thermodynamic model through the TeS® v.2 software to perform a parametric study of biomass gasification using air and steam as gasifying agents for the biomasses analyzed. Moreover, an analysis of the energy potential of these biomasses in energy recovery processes, within the framework of the circular economy concept, could be conducted.

Author Contributions: J.M.d.S.J., A.P.M. and L.D.G.C., project proposal; J.M.d.S.J., methodology development; J.M.d.S.J. and L.D.G.C., research and validation; J.M.d.S.J. and L.D.G.C., development of results; A.P.M., J.M.d.S.J., Y.C.S. and L.D.G.C., constant evaluation of results; A.P.M., I.A.M.Z., Y.C.S. and J.F.P.B., supervision and guidance throughout the development of the article. All authors have read and agreed to the published version of the manuscript.

Funding: This study was financed, in part, by the São Paulo Research Foundation (FAPESP), Brazil. Process Number 23/01072-7.

Institutional Review Board Statement: Not applicable.

Informed Consent Statement: Not applicable.

Data Availability Statement: The original contributions presented in this study are included in the article. Further inquiries can be directed to the corresponding author.

Acknowledgments: This study was financed, in part, by the São Paulo Research Foundation (FAPESP), Brazil. Process Number 23/01072-7.

Conflicts of Interest: The authors declare no conflicts of interest.

Nomenclatures

G	Total Gibbs energy.
l	Liquid phase.
s	Solid phase.
v	Vapor phase.
NC	Number of components.
NF	Number of phases.
n_i^k	Number of moles of component i in phase k; i = [1, 2, 3, . . ., NC]; k = [v, l, s].
R	Universal gas constant.
T	Temperature.
P	Pressure.
μ_i^k	Chemical potential of component i in phase k; i = [1, 2, 3, . . ., NC]; k = [v, l, s].
$\hat{f}_i^k$	Fugacity of component i in phase k.
f_i^o	Fugacity of pure species i in a standard reference state
a_{mi}	Number of atoms of element i in component m.
n_i^o	Number of moles in standard state.
H_i^k	Enthalpy of component i in phase k.
H_i^0	Enthalpy of component i in the standard state.
H^0	Total enthalpy.
Cp_i^k	Heat capacity of component i in phase k; i = [1, 2, 3, . . ., NC]; k = [v, l, s].
μ_i^0	Chemical potential of component i in a standard reference state.
$\hat{\varnothing}_i^k$	Coefficient of fugacity of component i in phase k; i = [1, 2, 3, . . ., NC]; k = [v, l].
y_i	Mole fraction of component i in the vapor phase.
x_i	Molar fraction of component i in the liquid phase.
a_i, b_i, c_i	Constants for calculating component saturation pressure i.
$A_{n,i}$	Constants for calculating the heat capacity of the component i in the vapor phase. i = [1, 2, 3, . . ., NC]; k = [1, 2, 3 and 4].
A_i, B_i, C_i, D_i	Constants for calculating the heat capacity of component i in the solid phase.
Z_i	Compressibility factor.
A, B, u, w	Parameters of the cubic equation of state.
a_m	Attraction parameter for mixtures.
b_m	Repulsion parameter for mixtures.
k_{ij}	Binary interaction parameter.
$T_{c,i}$	Critical component temperature i.
$P_{c,i}$	Critical component pressure i.

w_i	Acentric factor.
n	Number of moles.

References

1. Alfè, M.; Gargiulo, V.; Porto, M.; Migliaccio, R.; Pera, L.; Sellaro, M.; Pellegrino, C.; Abe, A.A.; Urciuolo, M.; Caputo, P. Pyrolysis and Gasification of a Real Refuse-Derived Fuel (RDF): The potential use of the products under a circular economy vision. *Molecules* **2022**, *27*, 8114. [CrossRef] [PubMed]
2. Araújo, D.J.C.; Machado, A.V.; Vilarinho, M.C.L.G. Availability and suitability of agroindustrial residues as feedstock for cellulose-based materials: Brazil case study. *Waste Biomass-Valorization* **2019**, *10*, 2863–2878. [CrossRef]
3. Reza, B.; Soltani, A.; Ruparathna, R.; Sadiq, R.; Hewage, K. Environmental and economic aspects of production and utilization of RDF as alternative fuel in cement plants: A case study of Metro Vancouver Waste Management. *Resour. Conserv. Recycl.* **2013**, *81*, 105–114. [CrossRef]
4. Cartagena; Colombia. Congreso de la República de Colombia. Emergencia Ambiental Inminente en Casi el 40% de los Rellenos Sanitarios en Colombia, Advierten Desde el Congreso Andesco. 2024. Available online: https://www.senado.gov.co/index.php/el-senado/noticias/13-senadores/5665-emergencia-ambiental-inminente-en-casi-el-40-de-los-rellenos-sanitarios-en-colombia-advierten-desde-el-congreso-andesco (accessed on 5 December 2024).
5. Basu, P. *Biomass Gasification and Pyrolysis: Practical Design and Theory*; Elsevier Inc.: New York, NY, USA, 2010; Chapter 5.
6. Sadhwani, N.; Adhikari, S.; Eden, M. Biomass gasification using carbon dioxide: Effect of temperature, CO_2/C ratio, and the study of reactions influencing the process. *Ind. Eng. Chem. Res.* **2016**, *55*, 2883–2891. [CrossRef]
7. Tang, H.; Kitagawa, K. Supercritical water gasification of biomass: Thermodynamic analysis with direct Gibbs free energy minimization. *Chem. Eng. J.* **2005**, *106*, 261–267. [CrossRef]
8. Khonde, R.; Hedaoo, S.; Deshmukh, S. Prediction of product gas composition from biomass gasification by the method of Gibbs free energy minimization. *Energy Sources Part A Recovery Util. Environ. Eff.* **2019**, *43*, 371–380. [CrossRef]
9. Moravvej, Z.; Bazargani, Z.; Esmaeilzadeh, F. Thermodynamic modeling and optimization of biomass and bio-renewable organic source gasification in supercritical water using gibbs free energy minimization. *Water* **2024**, *16*, 2123. [CrossRef]
10. Santos, J.M.D.; Mariano, A.P. Gasification of lignocellulosic waste in supercritical water: Study of thermodynamic equilibrium as a nonlinear programming problem. *Eng* **2024**, *5*, 1096–1111. [CrossRef]
11. Cui, H.; Turn, S.Q.; Tran, T.; Rogers, D. Mechanical dewatering and water leaching pretreatment of fresh banagrass, guinea grass, energy cane, and sugar cane: Characterization of fuel properties and byproduct streams. *Fuel Process. Technol.* **2015**, *139*, 159–172. [CrossRef]
12. Aluri, S.; Syed, A.; Flick, D.W.; Muzzy, J.D.; Sievers, C.; Agrawal, P.K. Pyrolysis and gasification studies of model refuse derived fuel (RDF) using thermogravimetric analysis. *Fuel Process. Technol.* **2018**, *179*, 154–166. [CrossRef]
13. Brotel, P.; Alves, E.; Borges, F.; Cardoso, M.; Codolette, J. Energy potential evaluation of different kinds of biomass. In Proceedings of the 7th International Colloquium on Eucalyptus Pulp, Vitória, Espirito Santo, Brazil, 26–29 May 2015.
14. Pashchenko, D. Thermodynamic equilibrium analysis of combined dry and steam reforming of propane for thermochemical waste-heat recuperation. *Int. J. Hydrogen Energy* **2017**, *42*, 14926–14935. [CrossRef]
15. Gambarotta, A.; Mironi, M.; Zubani, A. A non-stoichiometric equilibrium model for the simulation of the biomass gasification process. *Appl. Energy* **2018**, *227*, 119–127. [CrossRef]
16. Rocha, S.A.; Guirardello, R. An approach to calculate solid–liquid phase equilibrium for binary mixtures. *Fluid Phase Equilibria* **2009**, *281*, 12–21. [CrossRef]
17. Voll, F.A.P.; Rossi, C.C.R.S.; Silva, C.; Guirardello, R.; Souza, R.O.M.A.; Cabral, V.F.; Cardozo-Filho, L. Thermodynamic analysis of supercritical water gasification of methanol, ethanol, glycerol, glucose and cellulose. *Int. J. Hydrogen Energy* **2009**, *34*, 9737–9744. [CrossRef]
18. Hantoko, D.; Antoni; Kanchanatip, E.; Yan, M.; Weng, Z.; Gao, Z.; Zhong, Y. Assessment of sewage sludge gasification in supercritical water for H2-rich syngas production. *Process Saf. Environ. Prot.* **2019**, *131*, 63–72. [CrossRef]
19. Freitas, A.C.D.; Guirardello, R. Use of CO_2 as a co-reactant to promote syngas production in supercritical water gasification of sugarcane bagasse. *J. CO2 Util.* **2015**, *9*, 66–73. [CrossRef]
20. Jin, H.; Lu, Y.; Liao, B.; Guo, L.; Zhang, X. Hydrogen production by coal gasification in supercritical water with a fluidized bed reactor. *Int. J. Hydrogen Energy* **2010**, *35*, 7151–7160. [CrossRef]
21. Freitas, A.C.D.; Guirardello, R. Comparison of several glycerol reforming methods for hydrogen and syngas production using Gibbs energy minimization. *Int. J. Hydrogen Energy* **2014**, *39*, 17969–17984. [CrossRef]
22. Barros, T.V.; Carregosa, J.D.C.; Wisniewski, A., Jr.; Freitas, A.C.D.; Guirardello, R.; Ferreira-Pinto, L.; Bonfim-Rocha, L.; Jegatheesan, V.; Cardozo-Filho, L. Assessment of black liquor hydrothermal treatment under sub- and supercritical conditions: Products distribution and economic perspectives. *Chemosphere* **2022**, *286*, 131774. [CrossRef]
23. Sandler, S.I. *Chemical, Biochemical, and Engineering Thermodynamics*; John Wiley & Sons: Hoboken, NJ, USA, 2017.

24. Cox, K.R.; Chapman, W.G. The Properties of Gases and Liquids, 5th Edition By Bruce E. Poling (University of Toledo), John M. Prausnitz (University of California at Berkeley), and John P. O'Connell (University of Virginia). McGraw-Hill: New York. 2001. 768 pp. $115.00. ISBN 0-07-011682-2. *J. Am. Chem. Soc.* **2001**, *123*, 6745. [CrossRef]
25. Smith, J.M.; Van Ness, H.C.; Abbott, M.M.; Swihart, M.T. *Introduction to Chemical Engineering Thermodynamics*; McGraw-Hill: Singapore, 2018.
26. Kamath, R.S.; Biegler, L.T.; Grossmann, I.E. An equation-oriented approach for handling thermodynamics based on cubic equation of state in process optimization. *Comput. Chem. Eng.* **2010**, *34*, 2085–2096. [CrossRef]
27. Freitas, A.C.D.; Guirardello, R. Oxidative reforming of methane for hydrogen and synthesis gas production: Thermodynamic equilibrium analysis. *J. Nat. Gas Chem.* **2012**, *21*, 571–580. [CrossRef]
28. Santos, J.M.D.; De Sousa, G.F.B.; Vidotti, A.D.S.; De Freitas, A.C.D.; Guirardello, R. Optimization of glycerol gasification process in supercritical water using thermodynamic approach. *Chem. Eng. Trans.* **2021**, *86*, 847–852. [CrossRef]
29. Reddy, S.N.; Nanda, S.; Dalai, A.K.; Kozinski, J.A. Supercritical water gasification of biomass for hydrogen production. *Int. J. Hydrogen Energy* **2014**, *39*, 6912–6926. [CrossRef]
30. Basu, P.; Mettanant, V. Biomass Gasification in Supercritical Water—A Review. *Int. J. Chem. React. Eng.* **2009**, *7*, 32. [CrossRef]
31. Yan, Q.; Guo, L.; Lu, Y. Thermodynamic analysis of hydrogen production from biomass gasification in supercritical water. *Energy Convers. Manag.* **2006**, *47*, 1515–1528. [CrossRef]
32. Feng, W.; van der Kooi, H.J.; de Swaan Arons, J. Biomass conversions in subcritical and supercritical water: Driving force, phase equilibria, and thermodynamic analysis. *Chem. Eng. Process. Process Intensif.* **2004**, *43*, 1459–1467. [CrossRef]
33. Osada, M.; Yamaguchi, A.; Hiyoshi, N.; Sato, O.; Shirai, M. Gasification of sugarcane bagasse over supported ruthenium catalysts in supercritical water. *Energy Fuels* **2012**, *26*, 3179–3186. [CrossRef]
34. Molino, A.; Chianese, S.; Musmarra, D. Biomass gasification technology: The state of the art overview. *J. Energy Chem.* **2016**, *25*, 10–25. [CrossRef]
35. Moghaddam, E.; Goel, A.; Siedlecki, M.; Michalska, K.; Yakaboylu, O.; de Jong, W. Supercritical water gasification of wet biomass residues from farming and food production practices: Lab-scale experiments and comparison of different modelling approaches. *Sustain. Energy Fuels* **2021**, *5*, 1521–1537. [CrossRef]
36. Yakaboylu, O.; Harinck, J.; Smit, K.G.G.; de Jong, W. Supercritical water gasification of manure: A thermodynamic equilibrium modeling approach. *Biomass Bioenergy* **2013**, *59*, 253–263. [CrossRef]
37. Ma, W.; Jacobs, G.; Sparks, D.; Pendyala, V.; Hopps, S.; Thomas, G.; Hamdeh, H.; MacLennan, A.; Hu, Y.; Davis, B. Fischer-Tropsch synthesis: Effect of ammonia in syngas on the Fischer-Tropsch synthesis of precipitated iron catalyst. *J. Catal.* **2015**, *326*, 149–160. [CrossRef]
38. Munawar, M.; Ma, L.Q.; Haque, A.; Chen, W. *Advances in Bioenergy*; Chapter Five—Thermochemical conversions of municipal solid waste into fuels and chemicalsElsevier Inc.: Amsterdam, The Netherlands, 2023; Volume 8, pp. 239–305.
39. Chutichai, B.; Patcharavorachot, Y.; Assabumrungrat, S.; Arpornwichanop, A. Parametric analysis of a circulating fluidized bed biomass gasifier for hydrogen production. *Energy* **2015**, *82*, 406–413. [CrossRef]
40. Lu, Y.; Guo, L.; Zhang, X.; Yan, Q. Thermodynamic modeling and analysis of biomass gasification for hydrogen production in supercritical water. *Chem. Eng. J.* **2007**, *131*, 233–244. [CrossRef]
41. Pinto, F.; Franco, C.; André, R.N.; Miranda, M.; Gulyurtlu, I.; Cabrita, I. Co-gasification study of biomass mixed with plastic wastes. *Fuel* **2001**, *81*, 291–297. [CrossRef]
42. Houcinat, I.; Outili, N.; García-Jaran, B.; Sánchez-Oneto, J.; Portela, J.; Meniai, A. Renewable energy production and distribution. *Renew. Energy Prod. Distrib.* **2022**, *1*, 189–225.
43. Kitzler, H.; Pfeifer, C. Hofbauer. *Fuel Process. Technol.* **2011**, *92*, 908–914. [CrossRef]
44. Rambo, M.; Cardoso, A.; Bevilaqua, D.; Rizetti, T.; Ramos, L.; Korndörfer, G.; Martins, A. Silica from rice husk ash as an additive for rice plant. *J. Agron.* **2011**, *10*, 99–104. [CrossRef]
45. Rauch, R.; Hrbek, J.; Hofbauer, H. Biomass gasification for synthesis gas production and appilcations of the syngas. *WIREs Energy Environ.* **2013**, *3*, 343–362. [CrossRef]
46. Rostrup-Nielsen, J.; Christiansen, L.J. *Concepts in Syngas Manufacture*; World Scientific: Singapore, 2011; Volume 10.
47. Hernández, S.; Farkhondehfal, M.; Sastre, F.; Makkee, M.; Saracco, G.; Russo, N. Syngas production from electrchemical reduction of CO_2: Current status and prospective implementation. *Green Chem.* **2017**, *19*, 2326–2346. [CrossRef]